

## Validation of a finite-element solution for electrical impedance tomography in an anisotropic medium

This article has been downloaded from IOPscience. Please scroll down to see the full text article.

2007 Physiol. Meas. 28 S129

(<http://iopscience.iop.org/0967-3334/28/7/S10>)

View [the table of contents for this issue](#), or go to the [journal homepage](#) for more

Download details:

IP Address: 59.182.138.204

The article was downloaded on 05/05/2010 at 08:28

Please note that [terms and conditions apply](#).

# Validation of a finite-element solution for electrical impedance tomography in an anisotropic medium

Juan-Felipe P J Abascal<sup>1</sup>, Simon R Arridge<sup>2</sup>, William R B Lionheart<sup>3</sup>,  
Richard H Bayford<sup>4</sup> and David S Holder<sup>1,5</sup>

<sup>1</sup> Department of Medical Physics, University College London, London, UK

<sup>2</sup> Department of Computer Science, University College London, London, UK

<sup>3</sup> School of Mathematics, University of Manchester, Manchester, UK

<sup>4</sup> School of Health and Social Sciences, Middlesex University, London, UK

<sup>5</sup> Department of Clinical Neurophysiology, University College London, London, UK

E-mail: [j.abascal@cs.ucl.ac.uk](mailto:j.abascal@cs.ucl.ac.uk), [S.Arridge@cs.ucl.ac.uk](mailto:S.Arridge@cs.ucl.ac.uk), [bill.lionheart@manchester.ac.uk](mailto:bill.lionheart@manchester.ac.uk),  
[r.bayford@mdx.ac.uk](mailto:r.bayford@mdx.ac.uk) and [d.holder@ucl.ac.uk](mailto:d.holder@ucl.ac.uk)

Received 30 December 2006, accepted for publication 11 April 2007

Published 26 June 2007

Online at [stacks.iop.org/PM/28/S129](http://stacks.iop.org/PM/28/S129)

## Abstract

Electrical impedance tomography is an imaging method, with which volumetric images of conductivity are produced by injecting electrical current and measuring boundary voltages. It has the potential to become a portable non-invasive medical imaging technique. Until now, implementations have neglected anisotropy even though human tissues such as bone, muscle and brain white matter are markedly anisotropic. We present a numerical solution using the finite-element method that has been modified for modelling anisotropic conductive media. It was validated in an anisotropic domain against an analytical solution in an isotropic medium after the isotropic domain was diffeomorphically transformed into an anisotropic one. Convergence of the finite element to the analytical solution was verified by showing that the finite-element error norm decreased linearly related to the finite-element size, as the mesh density increased, for the simplified case of Laplace's equation in a cubic domain with a Dirichlet boundary condition.

Keywords: EIT, FEM, anisotropy, diffeomorphism

## 1. Introduction

### 1.1. Background

Different materials have dissimilar electrical conductivity; therefore, conductivity can be exploited to provide a volume map that differentiates materials of different electrical properties;

for example, for localizing water in the lung and cerebral blood volume change after visual or motor functional stimulation (Holder 2005). In electrical impedance tomography (EIT), the aim is to recover the conductivity inside an object by injecting electrical current and measuring voltage on the boundary (Borcea 2002). EIT for medical applications has been successfully applied to image gastric emptying (Mangall *et al* 1987), gastric acid secretion and lung ventilation (Metherall *et al* 1996, Harris *et al* 1988).

Recovering the volumetric conductivity from measured boundary voltages usually requires an accurate model that maps a given conductivity distribution onto a set of boundary voltages. This requires solution for the voltage in the whole domain, which at low frequencies can be modelled using the generalized Laplace's equation together with some boundary conditions (Paulson *et al* 1992, Somersalo *et al* 1992). A number of authors have proved uniqueness of the isotropic inverse conductivity problem (Kohn and Vogelius 1984, 1985, Sylvester and Uhlmann 1987). Nevertheless, anisotropic conductivities cannot be uniquely determined by boundary voltages (Lee and Uhlmann 2006) unless some *a priori* information is provided (Lionheart 1997) (see (Lionheart 2004, Borcea 2002) for reviews of EIT algorithms).

While it is well known that human tissues such as bone, muscle and brain white matter are anisotropic, most medical applications have hitherto neglected anisotropy although its modelling has been suggested for medical (Glidewell and Ng 1995, 1997) and geological (Pain *et al* 2003) applications. Avoiding correction for anisotropy of both white matter and skull has been found to lead to errors of about 10% on the electrical encephalogram forward solution and to be significantly relevant for inverse source localization (Wolters *et al* 2006, Wolters 2003), where the white matter anisotropic conductivity tensor was estimated from diffusion tensor magnetic resonance imaging (Hauelsen *et al* 2002) (Tuch (2002, Chapter 5). It seems plausible that modelling anisotropy is necessary to obtain an accurate forward solution for EIT of medical applications and that significant improvements in resulting image quality may result.

In an isotropic medium, Laplace's equation can be solved analytically for geometrically regular objects, for Neumann's boundary condition in a sphere using Green's functions (Kevorkian 2000), and for Dirichlet's boundary condition in an infinite plane by separation of variables (Weber and Arfken 2004). EIT for geometrically complicated objects can be solved numerically using the finite-element method (FEM) with 3D-EIDORS, a MATLAB toolbox for the 3D EIT problem with modelling of the electrodes (Polydorides and Lionheart 2002). We are not aware of any published analytical solution for an anisotropic medium. A FEM solution that modified EIDORS to model anisotropic media has been presented (Abascal and Lionheart 2004).

## 1.2. Theory

The field distribution is modelled by combining Maxwell's equations of electromagnetism that for the quasi-static approximation lead to generalized Laplace's equation in an anisotropic medium

$$\partial_i (\sigma_{ij} \partial_j u) = 0, \quad (1)$$

where  $\partial_i = \partial/\partial x_i$ , summation is understood over the repeated indices, and the conductivity  $\sigma$  is a symmetric 2-rank tensor

$$\sigma = \begin{pmatrix} \sigma_{11} & \sigma_{12} & \sigma_{13} \\ \sigma_{12} & \sigma_{22} & \sigma_{23} \\ \sigma_{13} & \sigma_{23} & \sigma_{33} \end{pmatrix}. \quad (2)$$

Thus, a voltage change on the  $j$ th direction yields a current density  $J$  which is not parallel to the applied field as given by

$$J_i = -\sigma_{ij}\partial_j u. \quad (3)$$

A weak formulation of generalized Laplace's equation obtained from Green's theorem is given by

$$\int_{\Omega} (\nabla v)^T (\sigma \nabla u) = \int_{\partial\Omega} v v^T (\sigma \nabla u), \quad (4)$$

where  $v$  is the unit outwards normal to the domain surface  $\partial\Omega$ , and  $u, v$  belong to the Sobolev space  $H^1(\Omega)$  (Braess 1997).

Boundary conditions for EIT that model the injected current at the boundary are based on the continuum Neumann condition (Cheney *et al* 1999)

$$\sigma \frac{\partial u}{\partial v} = J \quad \text{on } \partial\Omega. \quad (5)$$

A realistic model accounts for the electrodes contact impedance (Paulson *et al* 1992, Somersalo *et al* 1992). Other possible boundary conditions for Laplace's equation are the Dirichlet boundary condition

$$u = V \quad \text{on } \partial\Omega \quad (6)$$

or a combination of both conditions on different subsets of the boundary.

An important concept when dealing with the conductivity tensor rather than with scalar conductivity is that the voltage  $u(x)$  in the given domain  $\Omega$  with the conductivity  $\sigma(x)$  is equal to a new voltage  $\tilde{u}(\tilde{x})$  in the transformed domain  $\tilde{\Omega}$  with a transformed conductivity  $\tilde{\sigma}(\tilde{x})$ , under a diffeomorphism  $\Psi$ , i.e. a smooth and invertible transformation  $\Psi : \Omega \mapsto \tilde{\Omega}$ , such that  $\tilde{x} = \Psi(x)$ ,  $\tilde{u}(\tilde{x}) = u(\Psi^{-1}(\tilde{x}))$ , and  $\tilde{\sigma}$  is given by

$$\tilde{\sigma}(\tilde{x}) = \left( \frac{\Psi' \sigma \Psi'^T}{|\det(\Psi')|} \right) (\Psi^{-1}(\tilde{x})), \quad (7)$$

where  $\Psi'$  is the Jacobian of the diffeomorphism  $\Psi$  defined as  $\Psi' = \partial\tilde{x}/\partial x$ . This can be proved by defining the LHS of (4) as a bilinear function  $S_{\sigma}(u, v)$  and applying a diffeomorphism; one can verify that  $S_{\tilde{\sigma}}(\tilde{u}, \tilde{v}) = S_{\sigma}(u, v)$  for the above definition of  $\tilde{\sigma}$ .

### 1.3. Objective and design

The purpose of this paper is to expand and present a method for incorporation of anisotropy into a FEM forward solution originally presented in Abascal and Lionheart (2004) and to validate this empirically. The convergence of the anisotropic FEM solution to an isotropic analytical solution was tested by applying a diffeomorphic transformation to the isotropic domain that converted it into an anisotropic one. The Dirichlet boundary value problem was assumed for simplicity where the starting domain was a cube with isotropic conductivity, for which an analytical solution can be obtained by separation of variables. Convergence was verified in two steps: first, by the equivalence of the FEM isotropic and anisotropic solutions, and then by the convergence of the isotropic FEM onto the analytical solution while increasing the mesh density.

## 2. Methods

### 2.1. Model

Let  $\Omega$  be a homogeneous cubic domain of dimensions  $-1 \leq x \leq 1$ ,  $-1 \leq y \leq 1$ ,  $0 \leq z \leq 2$ , with isotropic conductivity  $\sigma = \text{diag}(1, 1, 1)$ . In this case, Laplace's equation (1) is simplified

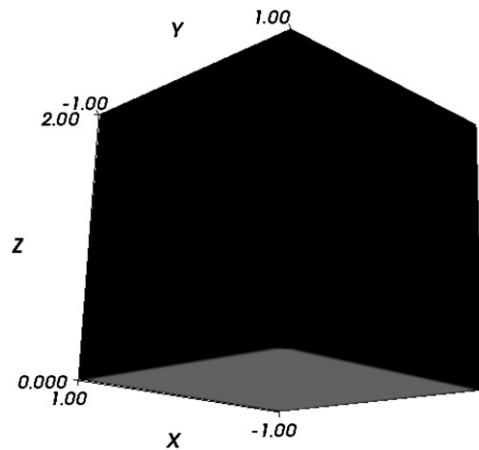


**Figure 1.** Imposed Dirichlet boundary condition: voltage  $u = 1$  on the plane  $z = 0$  for  $|x| < 1$ ,  $|y| < 1$  (grey), and  $u = 0$  on the rest of the boundary (black), for the isotropic domain (mesh of 98 843 elements).

as  $[\partial_{xx} + \partial_{yy} + \partial_{zz}]u(x, y, z) = 0$ . A Dirichlet boundary condition is assumed where the voltage is zero on the upper and side planes of the cube and one in the lower plane (figure 1), that is,

$$u(\pm 1, y, z) = 0 \quad (8)$$

$$u(x, \pm 1, z) = 0 \quad (9)$$

$$u(x, y, 2) = 0 \quad (10)$$

$$u(x, y, 0) = 1, \quad |x| < 1, \quad |y| < 1. \quad (11)$$

## 2.2. Analytical solution

An analytical solution to the Dirichlet's value problem can be solved by separation of variables (Weber and Arfken 2004)

$$u(x, y, z) = X(x)Y(y)Z(z). \quad (12)$$

Thus, by substituting  $u$  in Laplace's equation for an isotropic medium and reordering

$$\frac{1}{X} \frac{d^2 X}{dx^2} = -\frac{1}{Y} \frac{d^2 Y}{dy^2} - \frac{1}{Z} \frac{d^2 Z}{dz^2} = -r^2, \quad (13)$$

where  $r$  is a constant. A solution to  $X(x)$  can be expressed on the form

$$X(x) = A \cos(rx) + A' \sin(rx). \quad (14)$$

Since  $u(\pm 1, y, z) = 0$  for all  $y$  and  $z$ , then  $X(\pm 1) = 0$ , leading to  $A' = 0$  and  $r = l\pi/2$ , for  $l = 1, 3, \dots$ , which is equivalent to  $r = (2\mu + 1)\pi/2$ , for  $\mu = 0, 1, \dots$ . Therefore, the solution  $X(x)$  is the linear combination

$$X(x) = \sum_{\mu=0}^{\infty} A_{\mu} \cos \left[ (2\mu + 1) \frac{\pi x}{2} \right]. \quad (15)$$

Similarly for  $Y(y)$ , by reordering (13) for  $y$

$$\frac{1}{Y} \frac{d^2 Y}{dy^2} = r^2 - \frac{1}{Z} \frac{d^2 Z}{dz^2} = -s^2, \quad (16)$$

and imposing boundary conditions  $u(x, \pm 1, z) = 0$  for all  $x$  and  $z$ , then  $Y(\pm 1) = 0$ , leads to

$$Y(y) = \sum_{v=0}^{\infty} B_v \cos \left[ (2v+1) \frac{\pi y}{2} \right]. \quad (17)$$

A solution to  $Z(z)$  is obtained by reordering (16) for  $z$

$$\frac{1}{Z} \frac{d^2 Z}{dz^2} = r^2 + s^2 = t^2, \quad (18)$$

whose solution is of the form

$$Z(z) = C \exp(tz) + C' \exp(-tz), \quad (19)$$

where  $t$  is given by

$$t = t_{\mu\nu} = \frac{\pi}{2} \sqrt{(2\mu+1)^2 + (2\nu+1)^2}. \quad (20)$$

Applying the boundary conditions  $u(x, y, 2) = 0$  and  $u(x, y, 0) = 1$  for all  $x$  and  $y$  leads to

$$Z(z) = \frac{1}{1 - \exp(-4t_{\mu\nu})} (\exp(-t_{\mu\nu}z) - \exp(-t_{\mu\nu}(4-z))). \quad (21)$$

The solution to Laplace's solution is written by combining the coefficients  $A_\mu$  and  $B_\nu$  with  $D_{\mu\nu}$  as

$$u(x, y, z) = \sum_{\mu=0}^{\infty} \sum_{\nu=0}^{\infty} D_{\mu\nu} \cos \left[ (2\mu+1) \frac{\pi x}{2} \right] \cos \left[ (2\nu+1) \frac{\pi y}{2} \right] \\ \times \frac{1}{1 - \exp(-4t_{\mu\nu})} (\exp(-t_{\mu\nu}z) - \exp(-t_{\mu\nu}(4-z))). \quad (22)$$

The coefficients  $D_{\mu\nu}$  can be determined from the boundary condition  $u(x, y, 0) = 1$ ,

$$u(x, y, 0) = \sum_{\mu=0}^{\infty} \sum_{\nu=0}^{\infty} D_{\mu\nu} \cos \left[ (2\mu+1) \frac{\pi x}{2} \right] \cos \left[ (2\nu+1) \frac{\pi y}{2} \right] = 1. \quad (23)$$

Finally, the potential  $u$  is given by

$$u(x, y, z) = \sum_{\mu=0}^{\infty} \sum_{\nu=0}^{\infty} \frac{16(-1)^\mu (-1)^\nu}{\pi^2 (2\mu+1)(2\nu+1)} \cos \left[ (2\mu+1) \frac{\pi x}{2} \right] \cos \left[ (2\nu+1) \frac{\pi y}{2} \right] \\ \times \frac{1}{1 - \exp(-4t_{\mu\nu})} (\exp(-t_{\mu\nu}z) - \exp(-t_{\mu\nu}(4-z))). \quad (24)$$

### 2.3. FEM solution

The weak formulation of the generalized Laplace's equation with a Dirichlet boundary condition has zero current on the boundary. Let  $\phi_i$  be the shape function for the  $i$ th node, such that  $\phi_i = 1$  at node  $i$  and zero elsewhere, by replacing the test function  $v$  by the shape functions  $\phi_i$ , for all nodes, and expanding the voltage as  $u = \sum_j u_j \phi_j$ , where  $u_j$  is the voltage at node  $j$ , then the FEM formulation (4) becomes

$$\int_{\Omega} (\nabla \phi_i)^T \sigma \nabla u = \sum_j u_j \int_{\Omega} (\nabla \phi_i)^T \sigma \nabla \phi_j = 0, \quad (25)$$

which can be split into boundary  $\partial\Omega$  and interior  $\Omega \setminus \partial\Omega$  vertices,

$$\sum_{j \in \Omega \setminus \partial\Omega} u_j \int_{\Omega} (\nabla \phi_i)^T \sigma \nabla \phi_j = - \sum_{j \in \partial\Omega} u_j \int_{\Omega} (\nabla \phi_i)^T \sigma \nabla \phi_j. \quad (26)$$

It was computed as

$$A\mathbf{u} = 0, \quad (27)$$

where  $A$  is the system matrix, computed using a modified version of 3D-EIDORS that models anisotropic objects without considering the electrode contact impedance (Polydorides and Lionheart 2002, Abascal and Lionheart 2004), and  $\mathbf{u}$  is the potential on all vertices. Thus, by dividing the system matrix into blocks for the interior and exterior vertices

$$A\mathbf{u} = \begin{pmatrix} A_{11} & A_{12} \\ A_{21} & A_{22} \end{pmatrix} \begin{pmatrix} \mathbf{u}_{\Omega \setminus \partial\Omega} \\ \mathbf{u}_{\partial\Omega} \end{pmatrix}. \quad (28)$$

Since  $\mathbf{u}_{\partial\Omega}$  are the boundary conditions, the interior potential was solved as

$$A_{11}\mathbf{u}_{\Omega \setminus \partial\Omega} = -A_{12}\mathbf{u}_{\partial\Omega}. \quad (29)$$

#### 2.4. Convergence of the anisotropic FEM solution

**2.4.1. Convergence of the analytical solution.** For the computation of the analytical solution (24), one needs to select the maximum number of terms used to approximate an infinite series, given by  $\mu\nu$  for the maximum number of  $\mu$  and  $\nu$ , which here is  $n$ . The convergence of the analytical solution was analysed by computing the difference between the analytical voltage (24) and the imposed boundary condition (11), on the plane  $z = 0$  for  $|x| < 1$  and  $|y| < 1$ , for which  $u = 1$ , as a function of the number of terms  $n$ . The rest of boundary conditions (8)–(10), for which  $u = 0$ , were clearly satisfied.

**2.4.2. Comparison of isotropic and anisotropic FEM.** The FEM solution  $u^{\text{iso}}(x)$  in the isotropic domain  $\Omega$  with conductivity  $\sigma$ , as given by 3D-EIDORS (Polydorides and Lionheart 2002), was compared to the FEM solution  $u^{\text{ani}}(\tilde{x})$  in the transformed domain  $\tilde{\Omega}$  with conductivity  $\tilde{\sigma}(\tilde{x})$  (7) by

$$e_i^{\text{ani}} = 100 \frac{|u_i^{\text{iso}}(x) - u_i^{\text{ani}}(\tilde{x})|}{|u_i^{\text{iso}}(x)|}, \quad \text{for } i = 1, \dots, n_I \quad (30)$$

where  $n_I$  is the number of interior vertices since in the FEM Dirichlet boundary value problem the boundary potential is known (29).

A diffeomorphic transformation  $\Psi$  was applied to the domain  $\Omega$  by mapping the mesh vertices onto a new mesh in  $\tilde{\Omega}$ . The same mesh was used for simplicity to test that 3D-EIDORS (Polydorides and Lionheart 2002), and the modified version that models anisotropic objects (Abascal and Lionheart 2004), provided the same results; they should agree as the mesh density is increased. Two nonlinear transformations of a similar form differing only in the strength were applied. The strength of the transformation was measured by computing the absolute value of the determinant of the Jacobian of the transformation as a function of the domain,  $|\det(\Psi')| = |\det(\tilde{\sigma})|$ , which appears in (7) as a consequence of the transformation when one substitutes  $d\tilde{x} = |\det(\Psi')|dx$  in equation (4). The two transformations were

$$\begin{cases} \tilde{x} = 1.2 \exp(x) + 0.7y + 0.4z \\ \tilde{y} = -0.2x + 1.5 \exp(y) + 0.3z \\ \tilde{z} = -0.3x - 0.2y + 1.2 \exp(z) \end{cases} \quad (31)$$

$$\begin{cases} \tilde{x} = 13.8 \exp(x) + 15.7y + 18.4z \\ \tilde{y} = -0.2x + 23.5 \exp(y) + 0.3z \\ \tilde{z} = -0.3x - 0.2y + 9.2 \exp(z). \end{cases} \quad (32)$$

The transformed conductivity  $\tilde{\sigma}$  was computed elementwise by using (7) where  $\Psi'$  was calculated as follows. Let  $w$  be a vector in  $\Omega$ , its transformed vector  $\tilde{w}$  in  $\tilde{\Omega}$  is given by the push forward or Jacobian  $\Psi'$  as

$$\tilde{w} = \Psi' w. \quad (33)$$

In 3D,  $\Psi$  can be completely characterized by knowing the push forward of three independent vectors. Let  $r_i = (x_i, y_i, z_i)^T$  be the coordinates of the four vertices of a tetrahedron  $\Omega_k$ , for  $i = 0, 1, 2, 3$ , then taking  $r_0$  as a reference,  $W = [r_3 - r_0, r_2 - r_0, r_1 - r_0]$  is a 3-by-3 matrix whose columns are three independent vectors in  $\Omega_k$ . Similarly,  $\tilde{W} = [\tilde{r}_3 - \tilde{r}_0, \tilde{r}_2 - \tilde{r}_0, \tilde{r}_1 - \tilde{r}_0]$  is defined as a matrix whose columns are the transformed vectors in  $\tilde{\Omega}_k$  where  $\tilde{r}_i = (\tilde{x}_i, \tilde{y}_i, \tilde{z}_i)^T$ . Thus,  $\Psi'$  was computed elementwise as

$$\tilde{\Psi} = \tilde{W} W^{-1}. \quad (34)$$

**2.4.3. Convergence of the FEM solution.** Convergence of the FEM solution was studied by computing the discrepancy between the FEM and analytical solutions while increasing the mesh density. Two metrics were used for the comparison: the vertex relative error and the FEM error norm. Let  $u$  be the analytical solution and  $u^h$  the FEM solution, the percentage relative error was defined for each vertex as

$$e_i = 100 \left| \frac{u_i - u_i^h}{u_i} \right|. \quad (35)$$

The FEM error norm was approximated as

$$\|e\|_{\Omega} \simeq \left( \sum_{k=1}^N |e^{(k)}|^2 V_k \right)^{\frac{1}{2}}, \quad (36)$$

where  $N$  is the number of tetrahedra,  $V_k$  is the tetrahedral volume, and  $e^{(k)}$  is the absolute error of the  $k$ th tetrahedron  $\Omega_k$  computed as the vertex average:

$$e^{(k)} = \frac{1}{4} \sum_{i \in \Omega_k} |u_i - u_i^h|. \quad (37)$$

Defining the element size  $h$  as the largest edge in the mesh and imposing a bound on mesh quality, convergence was verified by studying the dependence of the FEM error on  $h$ ; we assumed convergence when the FEM error decreased by decreasing the element size. The mesh generator guaranteed a lower bound on the shape quality metric (Knupp 2003), of 0.2, with value 1 when the tetrahedron is equilateral and 0 when the tetrahedron is degenerate.

## 2.5. FEM mesh

The tetrahedral mesh for the FEM isotropic and anisotropic solutions comparison was generated using NETGEN (384 elements) (Schöberl 1997). For the comparison of the FEM with the analytical solution tetrahedral meshes of different mesh densities were created by using Cubit (2001, Sandia Corporation, <http://cubit.sandia.gov/>).

## 3. Results

### 3.1. Convergence of the analytical solution

The analytical solution converged slowly to the imposed Dirichlet condition (11), on the plane  $z = 0$  for  $|x| < 1$  and  $|y| < 1$ , for which  $u = 1$ , because of the voltage jump from  $u = 1$  to  $u = 0$  for  $|x| = 1$  and  $|y| = 1$  (figure 2). The difference was less than 0.01% for  $n = 1000$ , which was used for the rest of the analysis.

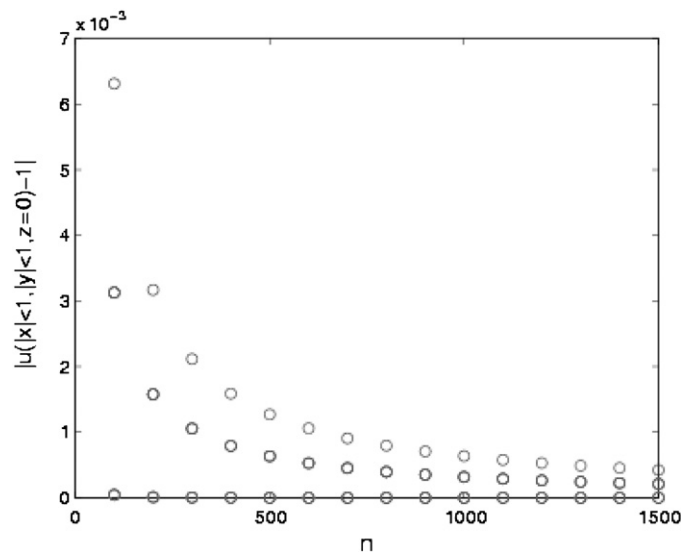


**Figure 2.** Convergence of the analytical solution (24),  $u$ , to the imposed boundary conditions  $u(x, y, z) = 1$ , for  $z = 0$ ,  $|x| < 1$ ,  $|y| < 1$  (11), versus the maximum number of terms  $\mu$  and  $\nu$  equal to  $n$  used to approximate the infinite series, for nine points at the specified region of the boundary, for which  $x$  and  $y$  take the values  $\pm 0.5$  and  $0$ , which led to the three different curves because of symmetry of the solution (24), for a mesh of 384 elements. For the rest of the analysis,  $1000^2$  terms ( $n = 1000$ ) were used to approximate  $u$ .

### 3.2. Comparison between the FEM isotropic and anisotropic solutions

The FEM anisotropic solution  $u(\tilde{x})$  in the transformed domain  $\tilde{\Omega}$  was verified to be equal (30), up to floating point accuracy, to the isotropic FEM solution  $u(x)$  in  $\Omega$ . The relative error is of the order  $10^{-13}\%$  for the nonlinear transformation (31) where errors were larger for those vertices for which the determinant of the Jacobian of the transformation  $\det(\Psi')$  was larger (figure 3(b)). Increasing the strength of the transformation (32), giving an increase of  $\det(\Psi')$  of several orders of magnitude (figure 3(c)) with respect to the previous one (figure 3(a)), led to a relative error of the order  $10^{-12}\%$  (figure 3(d)).

### 3.3. Comparison of analytical and FEM solutions

The FEM error norm  $\|e\|_{\Omega}$  decreased proportionally to the element size  $h$ , as the number of elements increased (table 1), following the relation  $\|e\|_{\Omega} \propto h^{\alpha}$  where a linear fit led to  $\alpha = 1.1$  with  $r = 0.98$  (figure 4). The maximum percentage relative error at each vertex did not decrease, as the mesh density increased (table 1), which may be due to the fact that the FEM solution cannot accurately model, for the given element size, the boundary conditions at the lower plane of the cube, at  $z = 0$ , where there is voltage jump from  $u = 1$  to  $u = 0$ . However, the FEM error norm that measures the total error decreased linearly.

## 4. Discussion

A method for an empirical validation of the FEM forward solution for Laplace's equation in an anisotropic medium has been presented. The convergence of the anisotropic FEM solution to an analytical solution was verified for the case of a homogeneous cube in terms of the relative vertex error and the FEM error norm. The isotropic solution in the given domain and

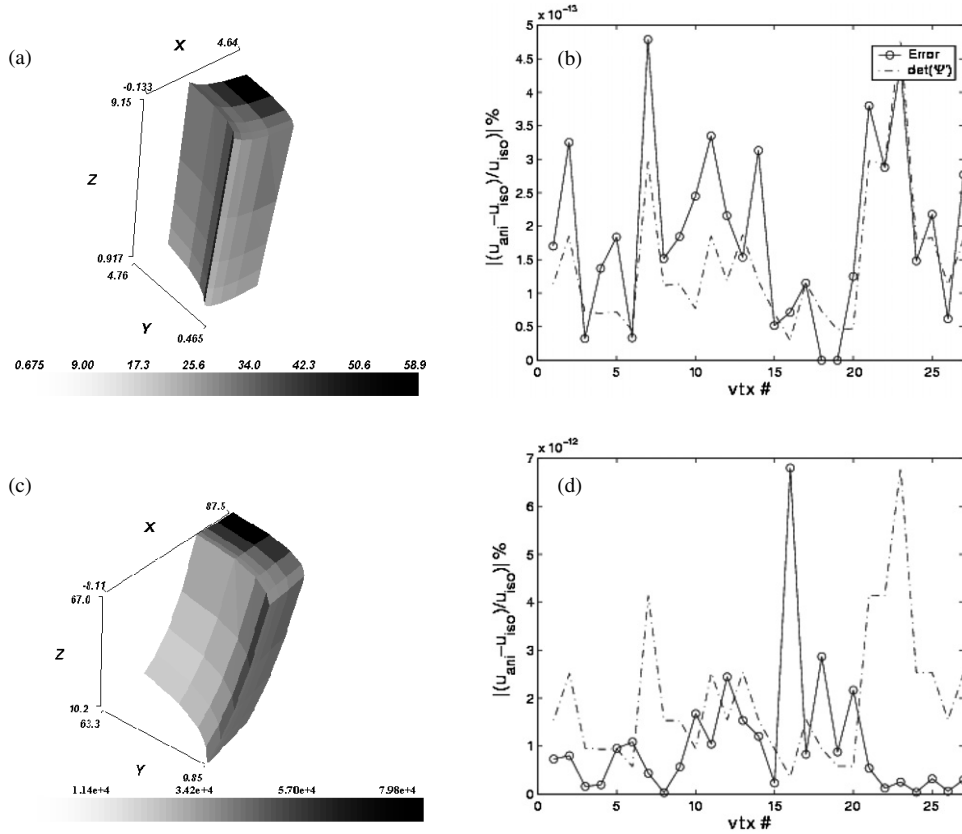


**Figure 3.** Percentage relative voltage difference  $e^{\text{ani}}$  (30) between the FEM isotropic solution  $u(x)$  in  $\Omega$  for  $\sigma = 1$  and the FEM anisotropic solution  $u(\bar{x})$  in the transformed domain  $\bar{\Omega}$  for  $\bar{\sigma}(\bar{x}) = \Psi' \sigma(x) \Psi'^T / |\det(\Psi')|$  (7), and absolute value of the determinant of the Jacobian of the transformation  $|\det(\Psi')|$  (dash line, which was scaled as  $|\det(\Psi')|(\max(e^{\text{ani}}) / \max(|\det(\Psi')|))$  to be plotted together with the relative error), for the interior vertices, where vtx no. is the number of interior vertices, under two nonlinear transformations given by (b) (31) and (d) (32). The term  $|\det(\Psi')| = |\det(\bar{\sigma})|$  measures the strength of the transformation where the transformation (a) (31) is of lower strength than the transformation (c) (32). (a)  $|\det(\Psi')|$  for the anisotropic domain given by the transformation (31). (b) Relative voltage difference (30) and normalized  $|\det(\Psi')|$  (dashed line) for the interior vertices. (c)  $|\det(\Psi')|$  for the anisotropic domain given by the transformation (32). (d) Relative voltage difference (30) and normalized  $|\det(\Psi')|$  (dashed line) for the interior vertices.

the anisotropic solution in the transformed domain have been shown to be equivalent for a nonlinear transformation. The FEM error norm decreased proportionally to the tetrahedral size. In contrast, the local relative vertex error did not decrease as the mesh density increased.

The goodness of the analytical solution was studied versus the number of basis functions in  $x$  and  $y$  used to approximate the infinite series. The error to fit the imposed boundary conditions was less than 0.01% when more than 1000 terms were employed. Since the number of terms in the series increases with the power of two of the number of basis functions, the analytical solution was approximated using 1000 basis functions. In addition, it presented a slow convergence because the imposed boundary conditions at the  $z = 0$  plane had a voltage jump from one, in the interior of the plane, to zero, at the edges. The error of the analytical

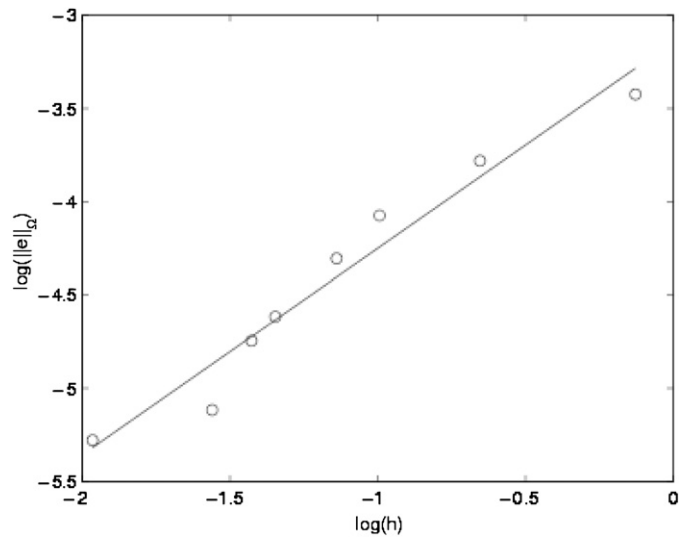


**Figure 4.** Log–log plot of the FEM error norm  $\|e\|_{\Omega}$  (36) versus the element size  $h$  (the same as in table 1) and a linear fit  $\|e\|_{\Omega} \propto h^{1.1}$  with correlation coefficient  $r = 0.98$ .

**Table 1.** FEM error norm  $\|e\|_{\Omega}$  (36) by increasing the number of elements  $N$ , which yielded a relation  $\|e\|_{\Omega} \propto h^{\alpha}$  (figure 4), where  $h$  is the element size; and the maximum percentage relative vertex error  $\max |e_i|$  (35).

$N$	% max $ e_i $	$\ e\ _{\Omega}$	$h$
495	35.69	0.0326	0.88
2 985	24.01	0.0228	0.52
8 025	34.93	0.0170	0.37
13 747	29.88	0.0135	0.32
35 864	28.13	0.0099	0.26
55 863	33.92	0.0087	0.24
98 843	25.78	0.0060	0.21
353 616	35.09	0.0051	0.14

solution was significantly smaller than the error between the analytical and FEM solutions, so the analytical solution was accurate enough for testing the FEM solution.

The extension to the EIT problem from these results, that is, considering Neumann's boundary conditions together with the electrode contact impedance, can be done since in EIT formulation the conductivity tensor appears only in the main part of the system matrix, which has been tested here.

The convergence of the anisotropic FEM solution to the analytical solution was studied in two steps. First, the FEM solution in the isotropic domain was equal up to floating point accuracy to the anisotropic FEM solution in the transformed domain under a nonlinear transformation. Because the difference was larger for the more distorted elements and by increasing the magnitude of the transformation, such that the determinant of the first derivatives of the transformation increased by several orders of magnitude, then the difference can be explained by the floating operations. Second, the FEM solution converged to the analytical solution with FEM error decreasing proportionally to the element size. However, the vertex error did not decrease accordingly, which could be due to the difficulty of the FEM solution

to model the boundary conditions for the considered element sizes. From the decrease of the FEM error, we can conclude that the FEM solution converged to the analytical solution.

The results verified that the anisotropic FEM solution is accurate enough for modelling the forward problem in an anisotropic medium. We plan to employ this approach in studying the influence of modelling anisotropy for EIT of the head, for which bone tissues such as the skull and white matter are anisotropic.

If, as in the case for inverse source modelling of the EEG (Wolters *et al* 2006, Wolters 2003), it transpires that modelling of anisotropy makes a significant difference, we plan to incorporate this into our forward model for linear (Bagshaw *et al* 2003) and nonlinear image reconstruction in ongoing trials of EIT in imaging in acute stroke (Romsauerova *et al* 2006), epileptic seizures (Fabrizi *et al* 2006) and fast electrical activity in the brain (Gilad *et al* 2005).

## Acknowledgment

The Epilepsy Research Foundation supported this study.

## References

- Abascal J F P-J and Lionheart W R B 2004 Rank analysis of the anisotropic inverse conductivity problem *Proc. ICEBI XII-EIT V (Gdansk, Poland)* pp 511–4
- Bagshaw A P, Liston A D, Bayford R H, Tizzard A, Gibson A P, Tidswell A T, Sparkes M K, Dehghani H, Binnie C D and Holder D S 2003 Electrical impedance tomography of human brain function using reconstruction algorithms based on the finite element method *NeuroImage* **20** 752–64
- Borcea L 2002 Electrical impedance tomography *Inverse Problems* **18** R99–R136
- Braess D 1997 *Finite Elements* (Cambridge, UK: Cambridge University Press)
- Cheney M, Isaacson D and Newell J C 1999 Electrical impedance tomography *SIAM Rev.* **41** 85–101
- Fabrizi L, Sparkes M, Horesh L, Abascal J F P-J, McEwan A, Bayford R H, Elwes R, Binnie C D and Holder D S 2006 Factors limiting the application of electrical impedance tomography for identification of regional conductivity changes using scalp electrodes during epileptic seizures in humans *Physiol. Meas.* **27** S163–74
- Gilad O, Horesh L, Ahadzi G M, Bayford R H and Holder D S 2005 Could synchronized neuronal activity be imaged using low frequency electrical impedance tomography (LF-EIT)? *6th Conf. on Biomedical Applications of Electrical Impedance Tomography (London, UK)*
- Glidewell M and Ng K T 1995 Anatomically constrained electrical-impedance tomography for anisotropic bodies via a two-step approach *IEEE Trans. Med. Imaging* **14** 498–503
- Glidewell M and Ng K T 1997 Anatomically constrained electrical impedance tomography for three-dimensional anisotropic bodies *IEEE Trans. Med. Imaging* **16** 572–80
- Harris N D, Suggett A J, Barber D C and Brown B H 1988 Applied potential tomography: a new technique for monitoring pulmonary function *Clin. Phys. Physiol. Meas.* **9** (Suppl. A) 79–85
- Hauelsen J, Tuch D S, Ramon C, Schimpf P H, Wedeen V J, George J S and Belliveau J W 2002 The influence of brain tissue anisotropy on human eeg and meg *NeuroImage* **15** 159–66
- Holder D S 2005 *Electrical Impedance Tomography* (London: IOP)
- Kevorkian J 2000 *Partial Differential Equations: Analytical Solution Techniques* (New York: Springer)
- Knupp P M 2003 Algebraic mesh quality metrics for unstructured initial meshes *Finite Elem. Anal. Des.* **39** 217–41
- Kohn R V and Vogelius M 1984 Determining conductivity by boundary measurements *Commun. Pure Appl. Math.* **37** 289–98
- Kohn R V and Vogelius M 1985 Determining conductivity by boundary measurements, interior results: II *Commun. Pure Appl. Math.* **38** 643–67
- Lee J M and Uhlmann G 2006 Determining anisotropic real-analytic conductivities by boundary measurements *Commun. Pure Appl. Math.* **42** 1097–112
- Lionheart W R B 1997 Conformal uniqueness results in anisotropic electrical impedance imaging *Inverse Problems* **13** 125–34
- Lionheart W R B 2004 EIT reconstruction algorithms: pitfalls, challenges and recent developments *Physiol. Meas.* **25** 125–42
- Mangall Y F, Baxter A, Avill R, Bird N, Brown B, Seager B D A and Johnson A 1987 Applied potential tomography: a new non-invasive technique for assessing gastric function *Clin. Phys. Physiol. Meas.* **8** 119–29

- Metherall P, Barber D C, Smallwood R H and Brown B H 1996 Three-dimensional electrical impedance tomography *Nature* **380** 509–12
- Pain C C, Herwanger J V, Saunders J H, Worthington M H and de Oliveira C R E 2003 Anisotropic and the art of resistivity tomography *Inverse Problems* **19** 1081–111
- Paulson K, Breckon W and Pidcock M 1992 Electrode modelling in electrical impedance tomography *SIAM J. Appl. Math.* **52** 1012–22
- Polydorides N and Lionheart W R B 2002 A Matlab toolkit for three-dimensional electrical impedance tomography: a contribution to the electrical impedance and diffuse optical reconstruction software project *Meas. Sci. Technol.* **13** 1871–83
- Romsauerova A, Ewan A M, Horesh L, Yerworth R, Bayford R H and Holder D S 2006 Multi-frequency electrical impedance tomography (EIT) of the adult human head: initial findings in brain tumours, arteriovenous malformations and chronic stroke, development of an analysis method and calibration *Physiol. Meas.* **27** S147–61
- Schöberl J 1997 NETGEN—an advancing front 2D/3D-mesh generator based on abstract rules *Comput. Vis. Sci.* **1** 41–52
- Somersalo E, Cheney M and Isaacson D 1992 Existence and uniqueness for electrode models for electric current computed tomography *SIAM J. Appl. Math.* **52** 1023–40
- Sylvester J and Uhlmann G 1987 A global uniqueness theorem for an inverse boundary value problem *Ann. Math.* **125** 153–69
- Tuch D S 2002 Diffusion MRI of complex tissue structure *PhD Thesis* Massachusetts Institute of Technology, Massachusetts
- Weber H J and Arfken G B 2004 *Essential Mathematical Methods for Physicists* (London, UK: Elsevier Academic)
- Wolters C H 2003 Influence of tissue conductivity inhomogeneity and anisotropy on EEG/EMG based source localization in the human brain *PhD Thesis* University of Leipzig, Leipzig, Germany
- Wolters C H, Anwander A, Tricoche X, Weinstein D, Koch M A and MacLeod R S 2006 Influence of tissue conductivity anisotropy on EEG/EMG field and return current computation in a realistic head model: a simulation and visualization study using high-resolution finite element modeling *NeuroImage* **30** 813–26